SciEn
Journal of Engineering Advancements Vol. 04(01) 2023, pp 25-34 https://doi.org/10.38032/jea.2023.01.005

Numerical Analysis on Cavitation-noise and Fluid-structure Interaction of AU-Outline GAWN Series and B-Series Marine Propellers

Md. Iftekharul Alam, Abidur Rahman Adib, Abdullah Al Rifat, Tafsirul Hassan, Md. Mizanur Rahman*

Department of Mechanical Engineering, Chittagong University of Engineering & Technology, Chattogram-4349, Bangladesh

Received: February 24, 2023, Revised: March 21, 2023, Accepted: March 23, 2023, Available Online: March 26, 2023

ABSTRACT

Cavitation and cavitation-induced noise are harmful to both marine propellers and marine wildlife. Thus, it is required to reduce cavitation in marine propellers by developing the best design marine propellers. Moreover, proper material should be selected during the construction of marine propellers to withstand high-pressure loads. This paper presents an evaluation of the hydrodynamic characteristics such as cavitation and cavitation-induced noise of AU-outline GAWN series and B-series marine propellers at 0˚, 5˚, 10˚, and 15˚ rake angles using Computational Fluid Dynamics (CFD) analysis. Moreover, the study aims to find out the optimized propeller material among Nickel-Aluminum-Bronze (NAB), S2 glass, Aluminum 6061, and carbon fiber reinforced plastic (CFRP) materials. It is concluded that the lowest cavitation noises are 153.3 dB and 153.1 dB at a 10° rake angle for AU-outline GAWN series and B-Series marine propellers respectively. S2 glass is observed to be the optimum material at low rake angles, while CFRP is the optimum material at high rake angles compared to all other potential materials for both AU-outline GAWN series and B-series propellers.

Keywords: Marine Propellers, AU-Outline GAWN Series, B-Series, Cavitation Noise, Rake Angle.

1 Introduction

Ships and marine vehicles are able to maneuver themselves in the water because of the propulsion forces they use. Marine propellers are rotating devices with several blades to produce linear thrust on the water to move the corresponding marine vehicles. For efficient propulsion, the proper design of marine propellers is required. Predicting and determining the propulsive efficiency of ship design at the pre-design stage is a need. The proper propeller blade design is a quite difficult task because it has to make sure the reduction of cavitation, noise, erosion, and increasing of its life while improving efficiency [1]. The process of designing a propeller is also limited by certain hydrodynamics factors, such as the Reynolds number and maximum diameter in the event of weight loading, among others [2]. Cavitation and cavitation-induced noises are also included as barriers in the case of proper designing of marine propellers. Conforming to Bernoulli's principle, cavitation is the formation of vapor bubbles in the water near a rotating propeller blade in areas of low pressure. There are several types of cavitation that occur in marine propellers such as bubble cavitation, sheet cavitation, cloud cavitation, tip and vortex cavitation, blade root cavitation, etc. [3]. There are two types of noise induced by the propeller, non-cavitating noise, and cavitation noise. Collapsing cavitation bubbles generate shock waves, which result in noise also known as cavitation noise. This is basically 'white noise' up to around 1 MHz in frequency. The amount of noise produced by a cavitating propeller is dependent on the kind of cavitation present at the time of operation [4]. The noise generated due to cavitation is more dangerous. The effect of marine propeller cavitation noise is higher than that of propeller non-cavitation noise [5]. Thus, the prediction and reduction of marine propeller cavitation noise is a must. Moreover, marine propellers must operate in saltwater, which is a corrosion-promoting environment. Thus, corrosion-resistant materials must be used in their production. Aluminum and stainless-steel alloys are the primary materials used in the manufacture of maritime propellers. Besides, there are also many other materials available to manufacture maritime propellers. The marine propeller designs must be such that those are with less cavitation and cavitation noise with higher pressure load sustaining. For designing and investigating marine propellers, there are different approaches such as numerical, analytical, experimental, etc. At present, numerical analysis of marine propellers such as computational fluid dynamics (CFD), structural analysis, etc. are becoming more popular besides experimental approaches. For example, Bosschers and Wijngaarden [6] conducted computational and experimental studies to predict the noise induced by cavitation. Three of the EU's SONIC project ship designs such as a cruise liner, a container vessel, and a catamaran designs were studied to observe how the noise from cavitation was predicted using computational and experimental techniques. It was found that the ETV-model provides acceptable agreement with the observed noise levels validated through full-scale trials on a cruise liner. The empirical model for sheet cavitation noise shows better results than the ETV model for a container vessel. The empirical result for a catamaran in MARIN's DWB showed significant variation that demands further investigation further. In overall, the prognostications of the ETV-model and the Brown-model belong to the range of observations. Bagheri et al. [7] carried a research work to analyze both cavitation and non-cavitating noise characteristics. Using the finite volume technique, they investigated the hydrodynamics and noise behavior of maritime propeller models (I and II) under a variety of operating circumstances. For the model I, it was observed that the cavitation fully occurred at J = 0.125 and the total SPL variations

*Corresponding Author Email Address: tafsir2086@gmail.com Published by: SciEn Publishing Group

between cavitating and non-cavitating conditions fluctuated between 15-40 dB. These results also vary from 4-20 dB for J = 0.125 and 0.166. For model II, cavitation occurred at J = 0.32 and total SPLs was calculated at J = 0.8, 0.6, 0.4, and 0.32 also. Total SPLs under cavitating conditions for N = 1850 rpm and J = 0.32 were found to be higher than total SPLs under non-cavitating conditions for N = 800 rpm and J = 0.4. Numerical research was conducted by Usta et al. [8] on the prediction of performance, cavitation, and erosion features of the King's College-D (KCD)-193 model marine propeller under various flow conditions. They used an unstable Detached Eddy Simulation (DES) turbulence model in conjunction with the Computational Fluid Dynamics (CFD) program STAR-CCM+. Three different approaches were used to model cavitation erosion on the propeller blades, with pressure, saturation pressure, the volume fraction of vapor, the time derivative of pressure, and time derivative of the volume fraction of vapor on the propeller blades obtained from simulations as input variables. The authors presented a novel method for predicting the severity of cavitation erosion on the propeller blade. Yamatogi et al. [9] studied composite materials for marine propellers while they were trying to develop a composite material made up of marine propellers having ship energy conservation. They examined the cavitation erosion of different types of composite materials and revealed that fibre-reinforced plastics (FRPs) were not resistant to the erosion caused by cavitation to which the marine propeller was subjected throughout the research. However, it was concluded that the erosion resistance of aluminum bronze (NAB), which is often used for maritime propellers, was much higher than that of any other FRPs. The erosion resistance of GFRPs was lower than that of CFRPs where AFRPs showed the strongest erosion resistance among FRPs. On further investigation, it was concluded that there were fibre bundles with resin in CFRPs, while there were few fibre bundles in the case of GFRPs and the fibres of GFRPs were longer than those of CFRPs. While designing four-bladed marine propellers, the study focused on engines producing 85 bhp and ships traveling at 30 knots, which were both considered to be high-performed [10]. Static analysis was accomplished on an aluminum composite propeller that was made up of a mix of R Glass, S2 Glass, and CFRP (Carbon Fiber Reinforced Plastics). It was decided to use different sections for the single blade utilizing HYDRO PROCAD, and using section coordinate data, a 3D 4-blade propeller was modeled in CATIA V5R20 and analysis was conducted using ANSYS. Again, investigators utilized DTMB 4119 marine propeller model in a series of computational tests that evaluated the Blade Stress while conducting operations in open water [11]. The blade axial strain and the propeller flow field distribution also had their corresponding stress distribution investigated. The data gathered from ANSYS FLUENT simulations provided very precise and trustworthy hydrodynamic load calculation results for the propeller construction.

There have been huge research works to develop and improve the design of marine propellers. Many series and types of marine propellers have been developed till now. However, all these modern designs of marine propellers are still in their infancy. Marine propeller materials are needed to avoid and sustain cavitation-induced damages and noises. There are many different parameters such as variation in the blade section, rake and skew angle change, material change, etc. to reduce the cavitation and its induced noise. Cavitation, corrosion, impact loading, cavitation-induced noises, biological invasions, fractures, and fatigue are some of the problems that marine propellers still face while operating. Thus, the aim of this research is to predict and investigate the hydrodynamic characteristics, cavitation, and cavitation-induced noise within proper boundary conditions by varying the rake angles of AU-outline GAWN series and B-series marine propellers. Another aim of this study is to choose the best material among Aluminum 6061 alloy, Nickel-Aluminum-Bronze (NAB), S2 glass, and carbon fibre-reinforced plastic (CFRP) materials based on structural criteria. Both series of marine propellers with the variation of rake angles of 0°, 5°, 10°, and 15° respectively have been modeled in PropCad 2005 and SOLIDWORKS 2020. The CFD and one-way FSI simulations were done in ANSYS 19.2. Finally, the results of both CFD and static structural analysis are compared with published literature.

2 Materials and Method

Firstly, AU-outline GAWN series and B-series marine propellers of the same diameter with the variation of rake angles of 0°, 5°, 10°, and 15° respectively (total 8 marine propellers) are modeled and combined in both PropCad 2005 and SOLIDWORKS 2020. Then cavitation, hydrodynamics characteristics, and cavitation-induced sound pressure level (SPL) are investigated in ANSYS FLUENT. The pressure loads are imported in static structural analysis and one-way fluid-structure interaction (FSI) is used with the variation of four different materials such as Aluminium 6061 alloy, Nickel-Aluminium-Bronze (NAB), S2 Glass, and carbon fiber reinforced plastic (CFRP). After the completion of the simulations, a comparison among the obtained results is done to determine the intended outcome.

2.1 Propeller models

Both PropCad 2005 and SOLIDWORKS 2020 software have been used in designing both AU-outline GAWN series and B-series marine propellers. At first, marine propeller blades have been modeled in PropCad and hubs of marine propellers have been modeled in SOLIDWORKS later. Both series of marine propellers have the same diameter of 0.304 m and rake angles of 0°, 5°, 10°, and 15° respectively. The marine propeller design properties for both series are given in Table 1.

Table 1 Design properties of marine propellers (AU-outline GAWN and B-series) [12].

Parameter	Value
Marine propeller diameter	0.3048 m
Number of marine propeller blades	5
Skew angle	0°
Expended area ratio	0.725
Nominal pitch	0.36576 m
Rake angles	0°, 5°, 10°, and 15°

Those general parameters were the same in the design of both AU-outline GAWN series and B-series marine propellers. By changing the rake angles of 0°, 5°, 10°, and 15° respectively for both series AU-outline GAWN series and B-series, a total of 8 marine propellers have been modeled.

2.2 Mathematical Models

2.2.1 The Navier-Stokes Equation

ANSYS FLUENT is a robust and sophisticated CFD tool which is a finite volume method-based tool. The Navier-Stokes equation is the governing equation of the CFD analysis which is a partial differential equation that defines the flow characteristics of incompressible fluid as given below:

Continuity equation:

$$\frac{\partial \rho}{\partial t}+\frac{\partial(\rho u)}{\partial x}+\frac{\partial(\rho v)}{\partial y}+\frac{\partial(\rho w)}{\partial z}=0 \tag{1}$$

Conservation of momentum:
In x-direction:

$$\frac{\partial(\rho u)}{\partial t}+\frac{\partial(\rho u^2)}{\partial x}+\frac{\partial(\rho uv)}{\partial y}+\frac{\partial(\rho uw)}{\partial z}=-\frac{\partial p}{\partial x}+\frac{1}{\mathrm{Re}}\left(\frac{\partial \tau_{xx}}{\partial x}+\frac{\partial \tau_{xy}}{\partial y}+\frac{\partial \tau_{xz}}{\partial z}\right), \tag{2}$$

In y-direction:

$$\frac{\partial(\rho v)}{\partial t}+\frac{\partial(\rho uv)}{\partial x}+\frac{\partial(\rho v^2)}{\partial y}+\frac{\partial(\rho vw)}{\partial z}=-\frac{\partial p}{\partial y}+\frac{1}{\mathrm{Re}}\left(\frac{\partial \tau_{xy}}{\partial x}+\frac{\partial \tau_{yy}}{\partial y}+\frac{\partial \tau_{yz}}{\partial z}\right), \text{ and} \tag{3}$$

In z-direction:

$$\frac{\partial(\rho w)}{\partial t}+\frac{\partial(\rho uw)}{\partial x}+\frac{\partial(\rho vw)}{\partial y}+\frac{\partial(\rho w^2)}{\partial z}=-\frac{\partial p}{\partial z}+\frac{1}{\mathrm{Re}}\left(\frac{\partial \tau_{xz}}{\partial x}+\frac{\partial \tau_{yz}}{\partial y}+\frac{\partial \tau_{zz}}{\partial z}\right). \tag{4}$$

2.2.2 2.2.2 The SST k-ω Turbulence Model

The SST k-ω turbulence model is a two-equation eddy-viscosity model which was modified by Menter [13] from standard k-ω model [14]. The SST k-ω model generates a little too much turbulence in regions with substantial normal strain, such as stagnation regions and regions with rapid acceleration. In contrast to a typical k-ϵ model, this tendency is significantly less pronounced. Due to adverse pressure gradient and strong curvature regions, the K-ω SST model has been selected in this study [15].

Kinematic eddy viscosity,

$$\upsilon_T=\frac{a_1 k}{max(a_1\omega, SF_2)} \tag{5}$$

Turbulence kinetic energy,

$$\frac{\partial k}{\partial t}+U_j\frac{\partial k}{\partial x_j}=P_k-\beta^* k\omega+\frac{\partial}{\partial x_j}\left[(\nu+\sigma_k\nu_T)\frac{\partial k}{\partial x_j}\right] \tag{6}$$

Specific dissipation rate,

$$\frac{\partial \omega}{\partial t}+U_j\frac{\partial \omega}{\partial x_j}=\alpha S^2-\beta\omega^2+\frac{\partial}{\partial x_j}\left[(\nu+\sigma_\omega\nu_T)\frac{\partial \omega}{\partial x_j}\right]+2(1-F_1)\sigma_{\omega 2}\frac{1}{\omega}\frac{\partial k}{\partial x_i}\frac{\partial \omega}{\partial x_i} \tag{7}$$

where,

$$F_2=\tan h\left[\left[max\left(\frac{2\sqrt{k}}{\beta^*\omega y},\frac{500\nu}{y^2\omega}\right)\right]^2\right],$$

$$P_k=min\left(\tau_{ij}\frac{\partial U_i}{\partial x_j},10\beta^* k\omega\right),$$

$$F_1=tanh\left\{\left\{min\left[max\left(\frac{\sqrt{k}}{\beta^*\omega y},\frac{500\nu}{y^2\omega}\right),\frac{4\sigma_{\omega 2}k}{CD_{k\omega}y^2}\right]\right\}^4\right\}$$

$$CD_{k\omega}=max\left(2\rho\sigma_{\omega 2}\frac{1}{\omega}\frac{\partial k}{\partial x_i}\frac{\partial \omega}{\partial x_i},10^{-10}\right),$$

$$\phi=\phi_1F_1+\phi_2(1-F_1),\alpha_1=\frac{5}{9},\quad \alpha_2=0.44,$$

$$\beta_1=\frac{3}{40},\quad \beta_2=0.0828,\quad \beta^*=\frac{9}{100},\sigma_{k1}=0.85,\quad \sigma_{k2}=1,$$

$$\sigma_{\omega 1}=0.5, and\ \sigma_{\omega 2}=0.856.$$

2.2.3 The Schnerr and Sauer Model (Cavitation Model)

Conforming to Bernoulli's principle, cavitation is the formation of vapor bubbles in the water near a rotating propeller blade in areas of low pressure. In order to calculate the pressure-induced phase transition of liquid into vapor and vice versa, the Schnerr-Sauer cavitation model [16] has been used in the study. In order to get the solution for a volume fraction, α, with an extra source term for evaporation and condensation, it needs to solve for a volume fraction, α, while adding an additional source term to the right-hand side of the Eq. (8).

$$\frac{\partial \alpha}{\partial t}+\nabla\cdot(\alpha\boldsymbol{U})=-\frac{\dot{m}}{\rho} \tag{8}$$

The continuity equation becomes,

$$\nabla\cdot\bar{\boldsymbol{U}}=\left(\frac{1}{\rho_v}-\frac{1}{\rho_l}\right)\dot{m} \tag{9}$$

Here, $\dot{m}$ is the rate of change of mass, and ρ denotes the density of the liquid-vapor mixture. A formula for the mass transfer rate between the liquid and vapor is required in order to close the system of equations. The method of Sauer and Schnerr seems to be advantageous since it gives the position of a single bubble after the equation of motion is applied which is given in Eq. (10).

$$\dot{m}=\frac{\rho_1\rho_v}{\rho}(1-\alpha)\alpha\frac{3}{R}\sqrt{\frac{2}{3}\frac{(p-p_v)}{\rho_l}} \tag{10}$$

2.2.4 The Ffowcs Williams-Hawkings (FW-H) Acoustic Analogy

The FW-H is a solution to the Lighthill equation that has been created by Ffowcs Williams, John E., and David L. Hawkings [17]. FW-H formulation is utilized in the FVM to extract the total SPLs in the far field, which is then employed in the FVM. Following the suggestion made by Brentner and Farassat [18], the solution to the FW-H equation in the time domain was given by Brentner and Farassat where the pressure field is defined as follows:

$$P'(\vec{x},t)=P'_T(\vec{x},t)+P'_L(\vec{x},t) \tag{11}$$

$$4\pi P'_T(\vec{x},t)=\int_{f=0}\left[\frac{\rho_o\frac{\partial v_n}{\partial t}}{r(1-M_r)^2}\right]_{ret}dS+\int_{f=0}\left[\frac{\rho_o\frac{\partial v_n}{\partial t}\left(r\frac{\partial M_1}{\partial t}\hat{r}_i+C_oM_r-C_oM^2\right)}{r^2(1-M_r)^3}\right]_{ret}dS \tag{12}$$

$$4\pi P_T'(\vec{x},t) = \frac{1}{C_0}\int_{f=0}\left[\frac{l_1\hat{r}_i}{r(1-M_r)^2}\right]_{ret} dS + \int_{f=0}\left[\frac{l_r - l_i M_i}{r^2(1-M_r)^2}\right]_{ret} dS + \frac{1}{C_0}\int_{f=0}\left[\frac{\rho_0 v_n(r\frac{\partial M_1}{\partial t}\hat{r}_i + C_o M_r - C_o M^2)}{r^2(1-M_r)^3}\right]_{ret} dS \quad (13)$$

Here, P' is the total acoustic pressure, which is made up of P_T' and P_L' which denote the different degrees of acoustic pressure caused by thickness and loading in relation to the monopole and dipole sound sources, respectively. Blade rotation and unstable sheet cavitation on blades, for example, are classified as monopole sources, while the fluctuation pressure on the blade surface is classified as a dipole. Where (r = |x(t) y(t)|) denotes the distance between receiver and source, whereas x and t denote the location of the sound receiver on the time axis and the time at which the sound has been received. y and t are also specified as the location and time of the source, respectively. To begin, the flow around the marine propeller is measured in order to identify the causes of noise. When the RANS equations are solved, it is possible to extract the flow field of the propeller from the FVM. As integral surfaces, f = 0, the surfaces of the marine propeller blades will be chosen as integral surfaces for use in the simulation.

2.2.5 Structural Analysis Equations

The pressure load delivered to the proposed marine propellers will be calculated using the one-way FSI technique in a steady condition. The following finite element equation for static analysis [11].

$$Ku = F \quad (14)$$

Here, K, u, and F are the stiffness matrix of the propeller, the displacement vector of the propeller node, and the imported pressure load applied on the propeller respectively.

The design will be safe if,

$$\sigma = \frac{1}{2}(\sigma_1 - \sigma_2) < \sigma_{\max}, \quad (15)$$

where, σ and $\sigma_{\max}$ are main shear stress and maximum principle stress, respectively. The Von Mises stress is [19],

$$\bar{\sigma} = \frac{1}{\sqrt{2}}\sqrt{(\sigma_1-\sigma_2)^2 + (\sigma_2-\sigma_3)^2 + (\sigma_3-\sigma_4)^2}. \quad (16)$$

The factor of safety is,

$$N_f = \frac{S}{\bar{\sigma}}, \quad (17)$$

where, S and $\bar{\sigma}$ are the strength of the material and von mises stress respectively.

In the case of ANSYS static structural analysis, fixed support is applied to the direction of the axis of the shaft. Then the pressure loads from the ANSYS FLUENT are imported for each of the marine propellers. The analysis settings are the same for each static structural simulation described in Table 2.

After completing all setup in ANSYS static structural analysis, simulations are run for each rake angle of 4 types of both AU-outline GAWN series and B-series marine propellers by varying the materials such as Aluminium 6061 alloy, Nickel-Aluminium-Bronze (NAB), S2 glass, and carbon fiber reinforced plastic (CFRP).

Table 2 Details of analysis settings in static structural analysis

Step Controls	Details
Number of Steps	1
Current Step Number	1
Step End Time	1 s
Auto Time Stepping	Program Controlled
Solver Controls	
Solver Type	Program Controlled
Weak Springs	Off
Solver Pivot Checking	Program Controlled
Large Deflection	Off
Inertia Relief	Off

2.3 ANSYS Fluent Approach-CFD Analogy

The modeled Au-outline GAWN series and B-series marine propellers with the variation of rake angles of 0°, 5°, 10°, and 15° respectively (total 8 marine propellers) have been imported to ANSYS FLUENT. The computational domains-Fluid enclosure domain and Propeller domain are shown in Fig. 1. These domains are the same for each series of marine propellers of various rake angles. The inlet and outlet flow regions are also shown here.

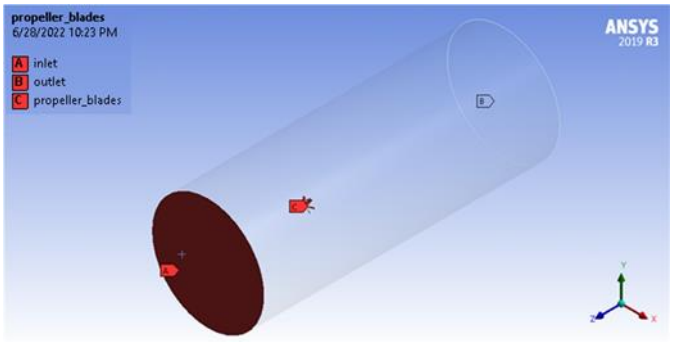

Fig. 1 General design of computational domains in FLUENT.

The inlet is placed at a distance of 2 m upstream from the propeller plane, and the outlet is placed at a distance of 4m downstream from the propeller plane. The domain dimensions considered are large enough to avoid external effects on the performance prediction of the propellers [20]. In the radial direction, the cylindrical domain has been kept at 1m in radius from the axis of the marine propeller hub. This has been the same for both AU-outline GAWN series and B-series marine propellers of rake angles of 0°, 5°, 10°, and 15° respectively. Before processing the solution in the Fluent solver, it is necessary to indicate fluid volumes and discretization of the infinite domain into a finite domain. Proper mesh generation is the key to accurate results. There are various types of mesh shapes-tetrahedral, quad-lateral, hexahedral, etc. In this study, tetrahedron mesh has been used for each series of modeled propellers of 4 types of rake angles. The mesh details are given in Table 3. A domain with a high grid number results in an accurate simulated result. However, the usage of a higher grid leads to high computational costs. It is observed that SPLs at 0° rake angle are approximately the same for the element number

higher than 6,50,000. Thus, the element number of the domain was chosen according to Table 3.

Table 3 Mesh details of modeled propellers in ANSYS Fluent.

Propellers	Rake Angles	Number of Nodes	Number of Elements
AU-outline GAWN Series	0°	128175	685436
	5°	120682	646999
	10°	121496	649404
	15°	121496	649404
B-series	0°	122112	653717
	5°	123456	661193
	10°	124033	663485
	15°	125791	672804

After proper meshing of modeled marine propellers, the FLUENT solver tool was used to get the solutions and results. The boundary conditions that have been used in ANSYS FLUENT are tabulated in Table 4. The data on boundary conditions have been collected from Helal et al. [21] for cavitation conditions. The inlet condition is velocity controlled. Thus, Reynolds number influences at the input and the body of the wall is defined as no slip condition. The boundary conditions and solver details are given in Table 4.

Table 4 Boundary conditions and solver details [21].

Parameter	Value
Solver type	Pressure-based
Process	Transient
Velocity formulation	Absolute
Rotation speed of the propeller, n	3000 rpm (50 rps)
Inlet velocity	8 m/s
Advance ratio, J	0.71
cavitation number, σ	1.763
Outlet pressure	207072 Pa
Vapor pressure	2337 Pa

The Schnerr-Sauer cavitation model [16] has been used in ANSYS Fluent as a cavitation model. The liquid water and vapor water have been defined as phase-1 and phase-2 in the multiphase model, respectively. For phase interaction, one mass transfer mechanism has been used. For this, the Schnerr-Sauer cavitation model is activated and the vapor pressure is defined as 2337 Pa. For the viscous model, the SST k-ω turbulence model is used. The Ffowcs Williams-Hawkings equation, which can be derived from the basic conservation laws of mass and momentum written in terms of generalized functions, represents the theoretical basis for the analysis of sound generated by a body moving in a fluid. It is worth noting that the velocity v for marine propeller applications is very small in comparison to the sound speed C0, and thus the Mach number M is close to zero. Thus, the transient flow field is statistically constant while using the Ffowcs Williams-Hawkings (FWH) acoustic model. This criterion must be maintained to perform an ANSYS FLUENT transient solution. Thus, it is recommended to execute an ANSYS FLUENT transient solution until the transient flow field is "statistically constant" while using the Ffowcs Williams-Hawkings (FWH) acoustic model. This implies that the whole set of relevant flow variables, along with the unsteady flow field under consideration, has been completely formed to the point that its statistics are stable throughout time. It is possible to assess if this condition has been satisfied by keeping an eye on the key flow variables at specific locations across the domain. In this present study, four hydrophone acoustic receivers are defined in FW-H acoustic model in ANSYS Fluent. Acoustic receivers 1 and 2 are defined at 550 mm away horizontally from the modeled propeller during simulation. Similarly, hydrophones 3 and 4 were defined at 1000 mm (1 m) away horizontally from the propeller. After the end of the CFD solution in ANSYS FLUENT, the results data is collected and the pressure load is imported to static structural analysis.

2.4 ANSYS Static Structural Analysis Approach (One-Way Fluid-structure Interaction)

In the ANSYS structural analysis, the geometries of both AU-outline series and B-series marine propellers of 4 types of rake angles are imported for static structural simulation processes.

After the completion of all setup in ANSYS static structural analysis, simulations have been run for each rake angle of 4 types for both AU-outline GAWN series and B-series marine propellers by varying the materials such as Aluminum 6061 alloy, Nickel-Aluminum-Bronze (NAB), S2 glass, and carbon fiber reinforced plastic (CFRP). The properties of those materials are tabulated in Table 5 and Table 6.

Table 5 Properties of accommodated materials.

Parameters	Materials		
	Aluminum 6061 [21], [22]	Ni-Al-Br (NAB) [23]	CFRP [24]
Density (kg/m^3)	2360	2485	7590
Young's Modulus (GPa)	47.78	86	125
Shear Modulus (GPa)	26	35.5	47.3
Bulk Modulus (GPa)	68.9	49.4	115
Poisson's Ratio	0.33	0.21	0.32
Yield Strength (MPa)	276	310	-
Ultimate Strength (MPa)	310	621	3790

Table 6 Properties of S2 Glass [10].

Parameters	S2 Glass
Density (kg/m^3)	1800
Young's Modulus x direction (MPa)	22925
Young's Modulus y direction (MPa)	22925
Young's Modulus z direction (MPa)	12400
Poisson's Ratio xy	0.12
Poisson's Ratio yz	0.2
Poisson's Ratio zx	0.2
Shear Modulus xy (MPa)	4700
Shear Modulus xz (MPa)	4200
Shear Modulus yz (MPa)	4200
Tensile Ultimate Strength (MPa)	4890

3 Results and Discussion

3.1 Vapor Volume Fraction (Cavitation)

Since cavitation is the formation of vapor bubbles in the water near a rotating propeller blade in areas of low pressure (suction side), the vapor volume fraction contours and data are also collected after the end of the CFD simulations via ANSYS CFD Post-processing tool. The changes in cavitation values for different rake angles are shown in Fig. 2.

3.2 Acoustic Results (Cavitation Noise)

The data on noises caused by cavitation is collected in the form of sound pressure level (SPL) graphs at the end of the CFD simulation in the CFD post-process tool. The SPL data of simulated various rake angles of both AU-outline GAWN series and B-series marine propellers are shown in Fig. 3 and Fig. 4.

The graphs of cavitation noise (SPL) are calculated for 500 Hz frequencies in 4 different positions of acoustic receivers of simulated 0°, 5°, 10°, and 15° rake angles of AU-outline GAWN series and B-series marine propellers.

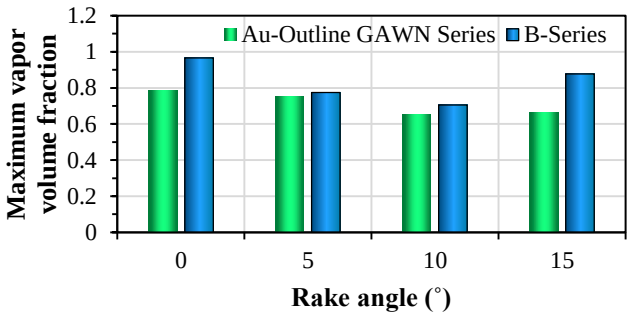

Fig. 2 Vapor fraction values for different rake angles

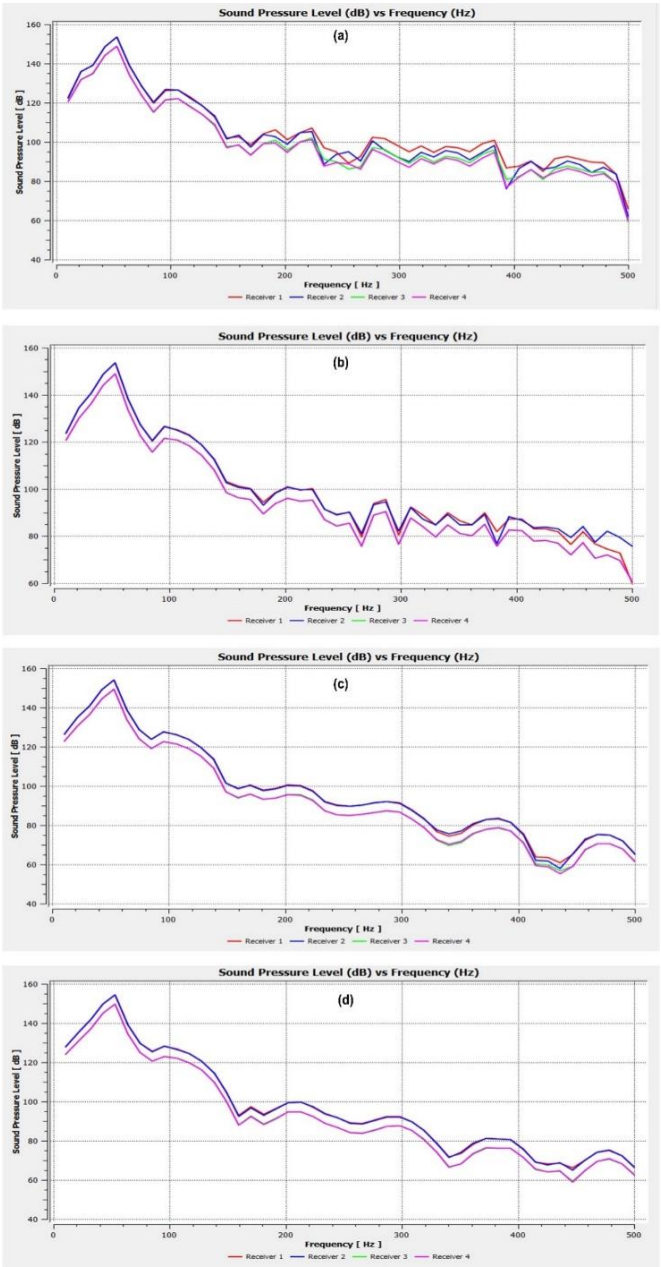

Fig. 3 Sound pressure level (dB) of (a) 0°, (b) 5°, (c) 10°, and (d) 15° rake angles of AU-outline GAWN series propellers

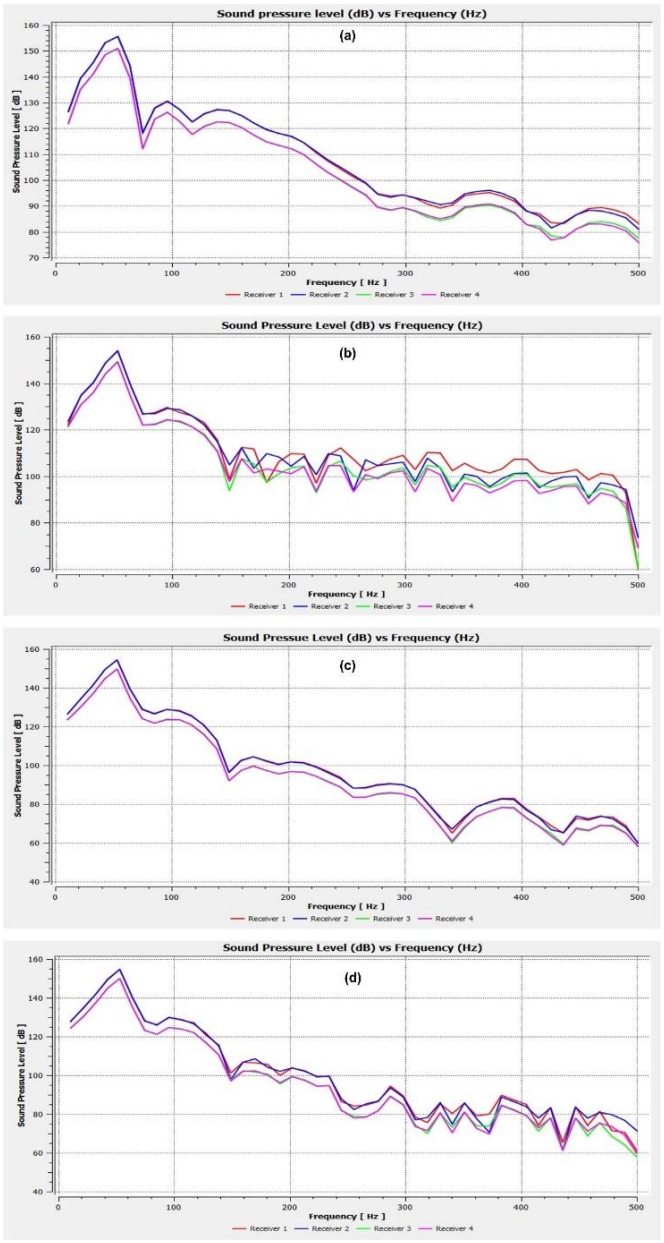

Fig. 4 Sound pressure level (dB) of (a) 0°, (b) 5°,(c) 10°, and (d) 15° rake angles of B-series propellers

The maximum sound pressure level (SPL) at 50 Hz frequency results are tabulated in Table 7 for both AU-outline GAWN series and B-series marine propellers.

Table 7 Maximum sound pressure level (dB) at 50 Hz frequency

Rake angles	0°	5°	10°	15°
AU-outline GAWN series	156.4 dB	154.2 dB	153.3 dB	157 dB
B-series	157.4 dB	155.9 dB	153.1 dB	156.6 dB

From the table, it can be observed that the lowest maximum sound pressure level (SPL) is found for 10° rake angle for both AU-outline GAWN and B-series marine propellers because the vapor volume fractions are the lowest at 10° rake angles of both AU-outline GAWN series and B-series marine propellers. The volume fraction values for the AU-outline GAWN series of marine propeller and B-series marine propeller are 0.653 and 0.705958 respectively at a 10° rake angle. The main sources of the sound pressure level are sheet cavitation since propeller geometry is one of the parameters that have effects on cavitation and its induced noise [25]. Thus, the rake angles of various propellers have different effects on cavitation noises. For this reason, changes in cavitation noises occur in different rake angles of propellers. For both AU-outline GAWN and B-series propellers, a 10° rake angle is found as the optimized rake angle with the lowest sound pressure level.

3.2.1 Static Structural Simulation Results

The pressure load generated from hydrodynamic characteristics influences the geometries of the blades and the hub of the propellers. In order to obtain the effects of materials, static structural simulation data is collected for 4 types of rake angles of both AU-outline GAWN series and B-series marine propellers for various materials such as Aluminum 6061 alloy, Nickel-Aluminum-Bronze (NAB), S2 glass, and carbon fiber reinforced plastic (CFRP). One-way FSI is used to obtain those data because only the effect of pressure load on the propellers and their materials has to be observed. The von-mises stresses for Aluminum 6061 alloy material are shown in Fig. 5 and Fig. 6 for AU-outline GAWN and B-series propellers, respectively.

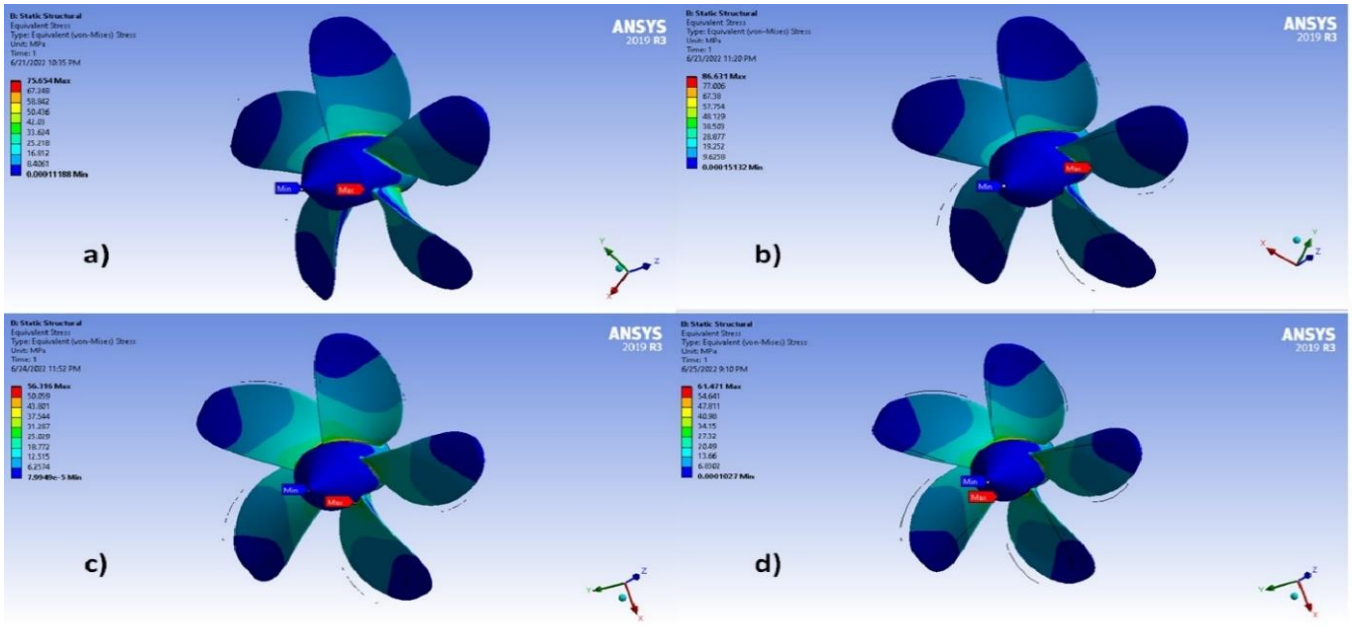

Fig. 5 Von-mises stresses of a) 0°, b) 5°, c) 10°, and d) 15° rake angles of AU-outline GAWN series propellers with Aluminum 6061 alloy material

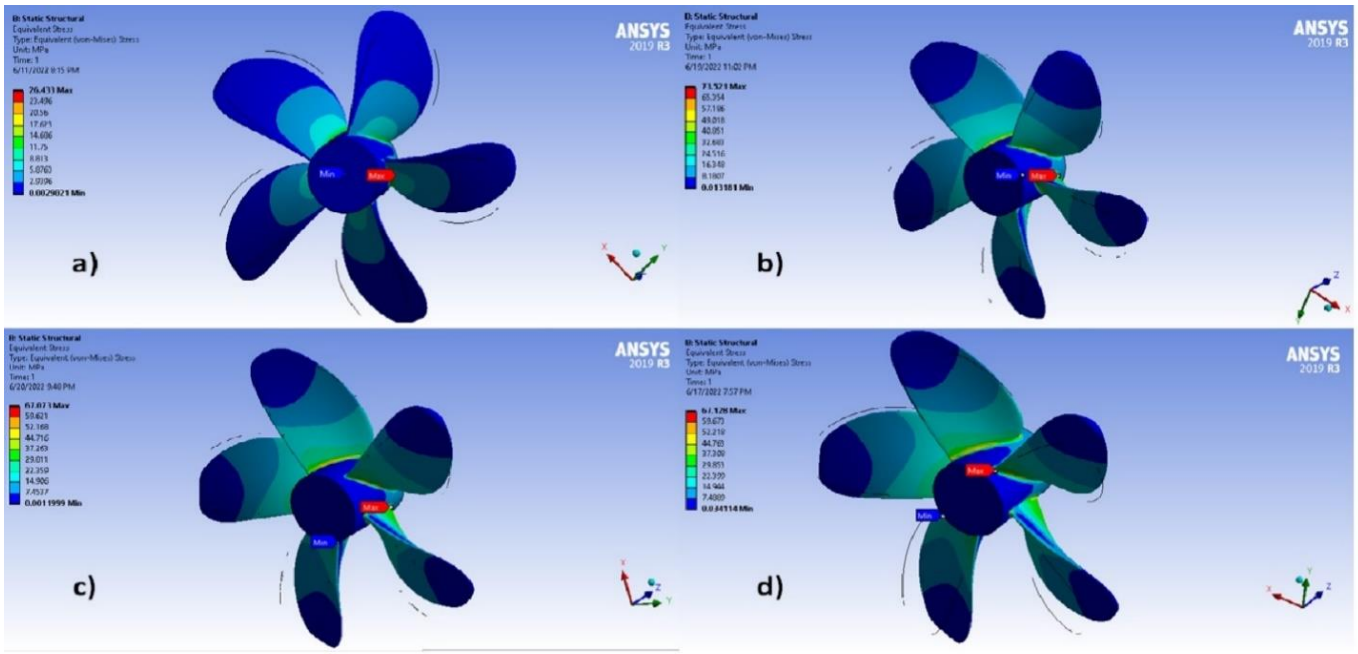

Fig. 6 Von-mises stresses of a) 0°, b) 5°, c) 10°, and d) 15° rake angles of B-series propellers with Aluminum 6061 alloy material

The effect of materials obtained for both AU-outline GAWN and B-series marine propellers of 0°, 5°, 10°, and 15° rake angles in static structural simulation. The best materials are chosen based on the lowest maximum Von-Mises stress results. Thus, the maximum von-mises stresses are demonstrated for AU-outline GAWN series and B-series marine propellers in Fig. 7 and Fig. 8, respectively. Aluminum 6061 alloy showed the lowest maximum von-mises stress among other materials. For example, Aluminum 6061 alloy material exhibited the lowest von-mises stress of 53.316 MPa at a 10° rake angle for AU-outline GAWN series marine propeller, while the Aluminum 6061 alloy material exhibited the lowest von-mises stress of 26.433 MPa at 0° rake angle for B-series marine propeller.

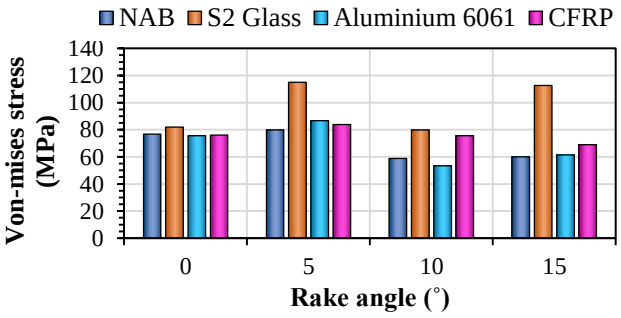

Fig. 7 Maximum Von-mises stresses for AU-outline GAWN series propellers

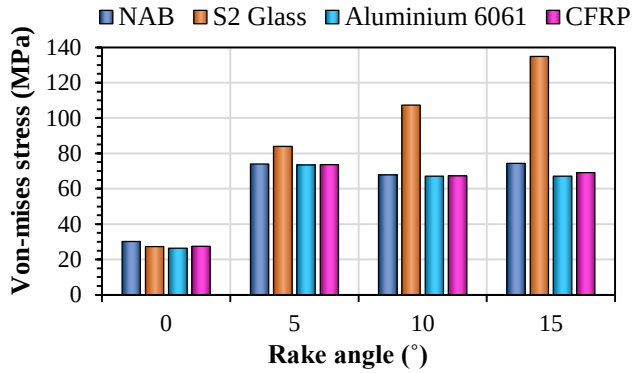

Fig. 8 Maximum Von-mises stresses for B-series propellers

The value of the factor of safety is demonstrated in Fig. 9 and Fig. 10, respectively. The maximum safety factor is observed for CFRP at a 10° rake angle for AU-outline GAWN series propeller. However, the maximum safety factor is observed for S2 glass at 0° rake angle for B-series marine propeller. The factor of safety for S2 glass is higher compared to other materials at low rake angles for both propellers, while the factor of safety for CFRP is higher compared to other materials at high rake angles for both propellers. Thus, S2 glass is the optimum material at a low rake angle for both propellers, while CFRP is the optimum material at a high rake angle for both propellers.

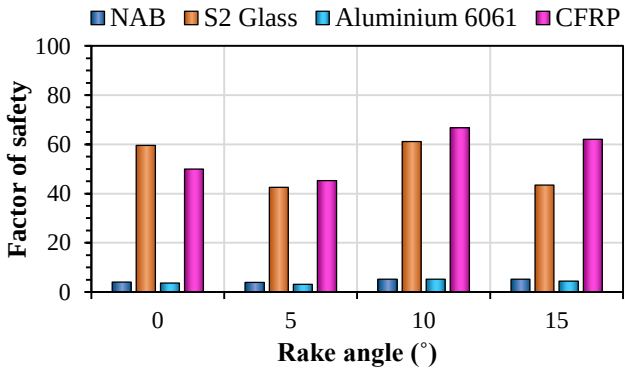

Fig. 9 Maximum factor of safety for Au-outline GAWN series propellers

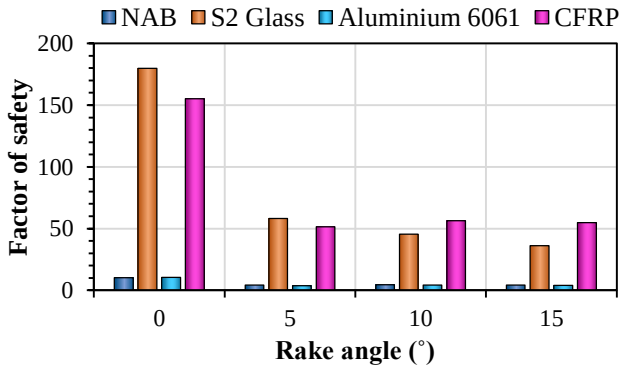

Fig. 10 Maximum factor of safety for B-series propellers

3.3 Comparison and Validation

The comparative results of sound pressure level (dB) up to 500 Hz frequency are illustrated in Fig. 11 with the Model II propeller in the article by Bagheri et al.[7] for a 0° rake angle. Fig. 11 shows that the variations with Bagheri et al. are 6.4 dB and 7.4 dB in maximum SPL for 0° rake angles of AU-outline GAWN and B-series propellers, respectively under cavitating conditions.

Another comparison of the simulated result of von-mises stress with Harish et al. [10] is illustrated in Fig. 12 for 0° rake angle for S2 glass and Aluminum 6061 alloy material in AU-outline GAWN and B-series propellers.

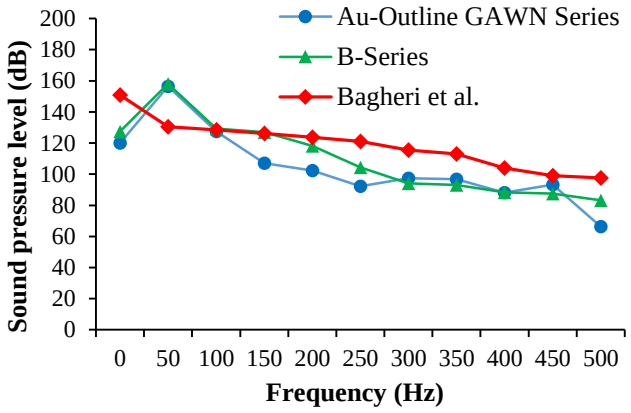

Fig. 11 Comparison of SPL with Bagheri et al. [7] for 0° rake angle.

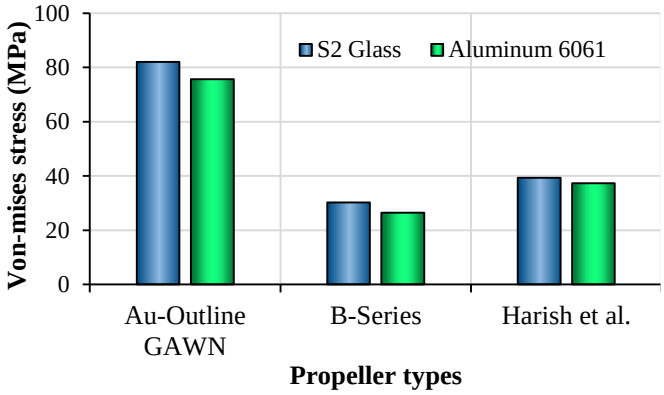

Fig. 12 Comparison of Von-mises stress with Harish et al. [10].

For S2 glass, the differences were 42.75 MPa and 9.069 MPa in AU-outline GAWN and B-series, respectively. For Aluminum 6061 material, the differences were 38.376 MPa and 10.845 MPa in AU-outline GAWN and B-series, respectively.

4 Conclusion

CFD analysis of both AU-outline GAWN series and B-series at 0°, 5°, 10°, and 15° rake angles reveals that the 10° rake angle for both series propellers is the most efficient because the cavitation and cavitation noise is the lowest in both AU-outline GAWN and B-series propellers at 10° rake angle. Moreover, upon conducting the static structural simulation in one-way fluid-structure interaction analysis, it is found that the von-mises stress values are lowest in the case of Aluminum 6061 alloy. However, S2 glass is the optimum material at low rake angles, while CFRP is the optimum material at high rake angles compared to all other potential materials for both AU-outline GAWN series and B-series propellers.

References

[1] Morgut, M. and Nobile, E., 2012. Influence of grid type and turbulence model on the numerical prediction of the flow around marine propellers working in uniform inflow. Ocean Engineering, 42, pp.26-34.

[2] Kerwin, J.E., 1986. Marine propellers. Annual Review of Fluid Mechanics, 18(1), pp.367-403.

[3] Abrahamsen, K., 2012, July 2012. The ship as an underwater noise source. In Proceedings of Meetings on Acoustics ECUA2012 (Vol. 17, No. 1, p. 070058). Acoustical Society of America.

[4] Wärtsilä Fixed Pitch Propellers. Available at https://www.wartsila.com/marine/products/propulsors-and-gears/propellers/wartsila-fixed-pitch-propellers. (Accessed 18 January, 2023.)

[5] Bertschneider, H., Bosschers, J., Choi, G.H., Ciappi, E., Farabee, T., Kawakita, C. and Tang, D., 2014. Specialist committee on hydrodynamic noise. Final report and recommendations to the 27th ITTC. Copenhagen, Sweden, 45.

[6] Lafeber, F.H., Bosschers, J. and van Wijngaarden, E., 2015, May. Computational and experimental prediction of propeller cavitation noise. In OCEANS 2015-Genova (pp. 1-9). IEEE.

[7] Bagheri, M.R., Seif, M.S., Mehdigholi, H. and Yaakob, O., 2017. Analysis of noise behaviour for marine propellers under cavitating and non-cavitating conditions. Ships and Offshore Structures, 12(1), pp.1-8.

[8] Usta, O., Aktas, B., Maasch, M., Turan, O., Atlar, M. and Korkut, E., 2017. A study on the numerical prediction of cavitation erosion for propellers. In Proceedings of the Fifth International Symposium on Marine Propulsors - SMP'17 12 - 15 June 2017, Espoo, Finland.

[9] Yamatogi, T., Murayama, H., Uzawa, K., Kageyama, K. and Watanabe, N., 2009, July. Study on cavitation erosion of composite materials for marine propeller. In 17th International Conference on Composite Materials Edinburgh, Scotland.

[10] Harish, B., Prasad, K.S. and Rao, G.U.M., 2015. Static Analysis of 4-Blade Marine Propeller. Journal of Aerospace Engineering & Technology, 5(2), pp.8-21.

[11] Yu, K., Yan, P. and Hu, J., 2020. Numerical analysis of blade stress of marine propellers. Journal of Marine Science and Application, 19, pp.436-443.

[12] Ghassemi, H., Gorji, M. and Mohammadi, J., 2018. Effect of tip rake angle on the hydrodynamic characteristics and sound pressure level around the marine propeller. Ships and Offshore Structures, 13(7), pp.759-768.

[13] Menter, F.R., 1994. Two-equation eddy-viscosity turbulence models for engineering applications. AIAA Journal, 32(8), pp.1598-1605.

[14] Wilcox, D.C., 1988. Reassessment of the scale-determining equation for advanced turbulence models. AIAA Journal, 26(11), pp.1299-1310.

[15] Hassan, T., Islam, M.T., Rahman, M.M., Ali, A.R.I. and Al Ziyan, A., 2022. Evaluation of different turbulence models at low reynolds number for the flow over symmetric and cambered airfoils. Journal of Engineering Advancements, 3(01), pp.12-22.

[16] Schnerr, G.H. and Sauer, J., 2001, May. Physical and numerical modeling of unsteady cavitation dynamics. In Fourth international conference on multiphase flow (Vol. 1). New Orleans, LO, USA: ICMF New Orleans.

[17] Ffowcs Williams, J.E. and Hawkings, D.L., 1969. Sound generation by turbulence and surfaces in arbitrary motion. Philosophical Transactions of the Royal Society of London. Series A, Mathematical and Physical Sciences, 264(1151), pp.321-342.

[18] Brentner, K.S. and Farassat, F., 2003. Modeling aerodynamically generated sound of helicopter rotors. Progress in Aerospace Sciences, 39(2-3), pp.83-120.

[19] Budynas, Richard Gordon and Nisbett JK and others, 2011. Shigley's mechanical engineering design. McGraw-Hill, New York.

[20] Hayati, A.N., Hashemi, S.M. and Shams, M., 2012. A study on the effect of the rake angle on the performance of marine propellers. Proceedings of the Institution of Mechanical Engineers, Part C: Journal of Mechanical Engineering Science, 226(4), pp.940-955.

[21] Helal, M.M., Ahmed, T.M., Banawan, A.A. and Kotb, M.A., 2018. Numerical prediction of sheet cavitation on marine propellers using CFD simulation with transition-sensitive turbulence model. Alexandria Engineering Journal, 57(4), pp.3805-3815.

[22] Seli, H., Awang, M., Ismail, A.I.M., Rachman, E. and Ahmad, Z.A., 2013. Evaluation of properties and FEM model of the friction welded mild steel-Al6061-alumina. Materials Research, 16, pp.453-467.

[23] ASM Material Data Sheet, Available at: http://asm.matweb.com/search/SpecificMaterial.asp?bassnum=MA2024T4. (Accessed on 12th November 2022).

[24] Uddin, M.M., Hossen, M.P., Jahan, M.M. and Islam, M.I., 2021, February. Structural analysis of composite propeller of ship using FEM. In AIP Conference Proceedings (Vol. 2324, No. 1, p. 030001). AIP Publishing LLC.

[25] Sharma, S.D., Mani, K. and Arakeri, V.H., 1990. Cavitation noise studies on marine propellers. Journal of Sound and Vibration, 138(2), pp.255-283.